DEVELOPMENT OF AN OPTICAL FIBER-BASED CORROSION DETECTION SENSOR BASED ON LASER LIGHT REFLECTION

by

MANJUNATHA SHENOY

Presented to the Faculty of the Graduate School of

The University of Texas at Arlington in Partial Fulfillment

of the Requirements

for the Degree of

MASTER OF SCIENCE IN MECHANICAL ENGINEERING

THE UNIVERSITY OF TEXAS AT ARLINGTON

May 2010

ACKNOWLEDGEMENTS

I would like to express my overwhelmed gratitude to Dr. Haiying Huang, who has the attitude and substance of a genius: she continually and convincingly conveyed a spirit of excitement in regard to research. Without her precious help and persistent guidance this thesis would not have been possible. I am grateful for providing me an opportunity to be a part of Advanced Sensor Technology Laboratory and also thank for the financial support extended for my studies.

I would like to thank Dr. Cheng Luo and Dr. Shih-Ho Chao for serving on my thesis committee. In addition, I would like to thank Mr. Kermit Beird, the machine shop supervisor, for his help and assistance during sensor fabrication.

I would like to thank and express my gratitude towards my parents and my beloved wife for their unending encouragement and constant support throughout my career.

April 16, 2010

ABSTRACT

DEVELOPMENT OF AN OPTICAL FIBER-BASED CORROSION DETECTION SENSOR BASED ON LASER LIGHT REFLECTION

Manjunatha Shenoy, M.S.

The University of Texas at Arlington, 2010

Supervising Professor: Haiying Huang

Corrosion plays a detrimental effect on the structural integrity of many engineering structures. It can compromise the safe operation of these structures by forming corrosion pits that deteriorates the structural surfaces and causes stress concentrations. Therefore, it is critical that corrosions are detected before structural integrity is compromised and repair becomes economically prohibitive. However, corrosions usually occur at intricate places that are hard to inspect visually. Manual inspection of the structures for corrosions requires dismantling the structures, which incurs high maintenance costs and could potentially cause damage to the components. One approach to reduce this cost is to detect and monitor corrosions using corrosion sensors that are capable of give an early indication of corrosion without requiring disassembly. Among various types of sensors, optical fiber sensors are particularly attractive because they are small, lightweight, easily multiplexed and most importantly, inexpensive to manufacture.

This thesis is focused on the development of an optical fiber corrosion sensor based on the principle of light reflection. The fabrication, analysis, and evaluation of the sensors are presented. The sensor consists of two parts, a sacrificial metallic film welded to a steel tube

using laser beam welding (tube/film subassembly) and an optical fiber sensor probe that measures the reflectivity of the sacrificial film. The side of the sacrificial film under inspection is finely polished and isolated from the environment while the other side of the sacrificial metallic film is exposed to the corrosive environment. Corrosion pits are first formed on the surface of the sacrificial film exposing to the environment and progress into the material as the exposure time increases. Once the corrosion pits penetrate through the thickness of the sacrificial film, the surface reflectivity of the polished side of the film decreases, resulting in a reduction in the amount of light collected by the sensor probe. Therefore, this corrosion-induced reflectivity decrease can be detected by monitoring the intensity of the sensor output, which serves as an indicator of the corrosion development. Since the corrosion sensor detects the presence of corrosion pits only when the corrosion is severe enough to penetrate through the thickness of the sacrificial film, the sensitivity of the corrosion sensor is therefore determined by the thickness of the sacrificial film. A flexible manufacturing technique was developed to assemble the sensor probe and the tube/film subassembly in a compact water-proof package. A multiplexing scheme that enables monitoring multiple sensors using a single set of instruments was also developed. The packaged corrosion sensors were evaluated by submerging them in saline solutions of different concentrations. The relationship between the optical power of the collected light and the corrosion development were characterized. Experimental results, analysis, and suggestions for future improvements are presented.

TABLE OF CONTENTS

LIST OF ILLUSTRATIONS

Figure Page

LIST OF TABLES

CHAPTER 1

INTRODUCTION

1.1 Importance of corrosion and optical fiber sensors

Corrosion is an important factor that limits the life of many metallic structures and it is one of the primary means by which materials deteriorate, especially in humid and saline environment. Corrosion is an accumulative process that alters the surface property and fracture strength of structures, resulting in premature deterioration. As the structural components ages, the occurrence of corrosions increases. In addition, corrosion occurrence is independent of usage. Inspection for corrosions is time consuming, costly and often causes additional damages since corrosions mostly occur at inaccessible locations that cannot be inspected visually[1]. Corrosion is a persistent problem that can only be managed but not eliminated. The impacts on cost saving and safety assurance would be significant if hidden corrosions can be detected without disassembly.

Conventional corrosion monitoring methods, such as weight loss coupons, iron counts, review of historical failure data, electrical resistance (ER) probes, and linear polarization resistance (LPR), have many limitations, including high cost of a separate infrastructure, large commitment of time and labor, and they could not give full and accurate information about the whole corrosion situation of the object being monitored. Optical fiber based sensors are a promising technology for corrosion monitoring as they are capable of non-destructive testing (NDT) and also offer a large number of attractive features such as small size, flexibility, negligible weight and are highly sensitive and immune to electromagnetic interference. More importantly, they are resistant to corrosive and hazardous environments, making them ideal for health monitoring of structures.

1.2 Literature review

Several researchers have presented different types of optical fiber corrosion sensors; Dong et al. developed a corrosion sensor wherein the fiber cladding was removed and replaced with a metal cladding having the basic composition of the structures. When the section of the cladding is replaced by a metal film, the core/cladding boundary becomes that of a dielectric/conductor, the total internal reflection boundary disappears at that point, and the light propagating in the core of this fiber is mostly absorbed by the metal cladding. As corrosion develops, the thickness decrease of the metal cladding reduces the light absorption and thus causes the output power to increase. Therefore the rate and the degree of corrosion can be monitored based on the change in the optical power output[2]. Li et al., Dong et al., and Himour et al. also developed similar optical fiber corrosion sensors wherein the fiber cladding was removed and the fiber core was coated with different metallic elements[3] [4] [5]. The metallic elements were deposited on the core of the fiber by different deposition techniques like physical vacuum deposition (PVD), electroplating, etc. Optical fiber long period grating (LPG) sensor coated with polyethylene oxide (PEO) was fabricated by Cooper et al[6]. The development of corrosion changes the refractive index of the PEO, resulting in a measurable change in the transmission spectrum of the LPG sensor, which was employed for corrosion detection of aging aircrafts. Several other researchers, e.g. Greene et al., and Dong et al., also designed optical fiber LPG sensors with different affinity coatings that are sensitive to the environmental parameters[7] [8]. The main drawback of using the uncladded optical fibers or the optical fiber LPG sensors is that the optical fiber cladding layer has to be removed, which makes the sensors fragile. In addition, all of the above mentioned optical fiber corrosion sensors are transmission type that requires the access of optical fiber at both ends. In contrast, reflection type optical fiber corrosion sensors are much simpler to use and install because of their compact size and simple wire arrangement. A reflection optical fiber corrosion sensor was developed by Qiao et al. by depositing Fe-C alloy sensing film on the end of the fiber[9]. The

sensors were then immersed in the saline solution and corrosion was detected from the change in the reflected light. Electroless plating deposition and DC magnetron sputtering are the two methods used to prepare the reflective sensing film. Several researchers including Dantan et al., Werner and Wolfbeis, Kermis et al., Mendoza et al. have also developed reflection type chemical sensors that are sensitive to the pH value changes in the steel reinforced structures based on absorption or fluorescence measurement[10] [11] [12] [13]. Corrosion is detected if the pH value of the concrete matrix decreases due to the deterioration of the calcium hydroxide layer on the steel surfaces. Lo et al. developed a corrosion sensor using a clad-etched fiber with a pair of fiber Bragg gratings which uses reflective multiplexing to predict corrosion[14]. Corrosion detection was also realized by monitoring the color shift in the incident broadband light reflected from the surface under inspection[15]. The fibers are coated with special sol-gel compounds, along with fluorescein as their base agent, for chloride detection. The chloride changes the color locally. The amount of colorshift both in terms of wavelength and in terms of intensity, determines the amount of corrosion present. Ganesh et al., Gobi et al. presented a new approach wherein the corrosion of metals was detected based on light scattering[16] [17] [18]. They have discussed that the rate of corrosion can be estimated by weight loss method, i.e. measure the initial and final weight of metal coupon after a certain period of exposure. They discussed about adapting a reference curve of corrosion rate versus surface roughness in order to predict either one value if the other value is known. Filho et al. proposed a sensor system which is multipoint and can detect corrosion several kilometers away using the optical time domain reflectometry (OTDR) [19] [20]. The OTDR detects the light reflected by each sensor head. The presence of corrosion was observed by the controlled etching of aluminum film which results in a change of light reflected from the aluminum film. The reflection decreases as the metal (aluminum) gets etched and the etch rate can be obtained from the OTDR traces. In general, for most of the corrosion sensing mechanisms discussed above, it is difficult to

correlate the actual corrosion experienced by the structures to the corrosion measured by the sensors.

1.3 Objective

The main objective of this thesis work is to develop an optical fiber based corrosion detection sensor that overcomes the limitations of conventional corrosion detection techniques that measure corrosion by-products in the vicinity of the corroded structures or measure the corrosion of a sacrificial material that has very different composition and corrosion characteristics as the structure material.

The advantages of the proposed sensor are:

1) Packaging technique – One of the main advantages of the proposed sensor is its flexible packaging technique. Because the sacrificial material can be exactly the same as that of the structural components, it makes correlating the corrosion of the sacrificial material with the structural corrosions much simpler. The sensor package is very compact and robust.
2) Reflective type sensor – The proposed sensor is a reflective type sensor which overcomes the main disadvantage of fragility associated with the transmission type corrosion detection sensors. In addition, it facilitates sensor multiplexing with OTDR.
3) Sensitivity and accuracy – The sensitivity and accuracy of the proposed sensor can be easily adjusted by varying the thickness of the sacrificial film. Using a set of sensors with different film thicknesses, the progression of corrosion can be monitored.
4) Fabrication – The fabrication technique of the proposed sensor is very simple and inexpensive.

1.4 Thesis outline

In this thesis, the development and characterization of an optical fiber corrosion sensor are discussed. Chapter 2 provides background information about corrosion and optical fibers. Chapter 3 explains the principle of operation of the optical fiber corrosion sensor. Chapter 4 discusses the corrosion sensor fabrication, testing, and result analysis. Chapter 5 focuses on the improvements of corrosion sensor by reducing the exposed area of the sacrificial film and its results are discussed. The summary of the work and the discussion of future work are presented in chapter 6.

CHAPTER 2

THEORY

2.1 Corrosion

Corrosion is the disintegration of an engineered material into its constituent atoms due to chemical reactions with its surroundings[21]. Similar to a battery, power generation in corrosion is an electrochemical reaction composed of two half cell reactions, i.e. an anodic reaction and a cathodic reaction. The corrosion cell can be represented as shown in Figure 2.1. The anodic reaction releases electrons while the cathodic reaction consumes electrons. The metallic surface exposed to the aqueous electrolyte possesses sites for an oxidation (anodic chemical reaction) that produces electrons in the metal, and a reduction (cathodic reaction) that consumes the electrons produced by the anodic reaction. These sites together make up a corrosion cell. The anodic reaction is the dissolution of the metal to form either soluble ionic products or an insoluble compound of the metal. The cathodic reaction is the reduction of dissolved oxygen gas or the reduction of solvent (water) to produce hydrogen gas.

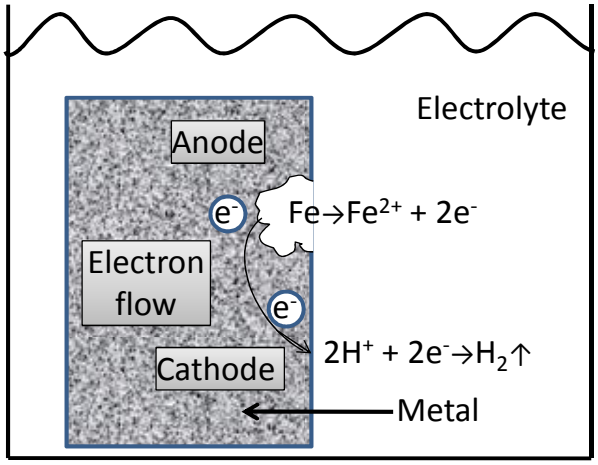

Figure 2.1: Corrosion process of carbon steel.

Carbon steel is one of the most widely used engineering materials. Corrosions of carbon steel can be categorized as:

- General corrosion – Also known as uniform corrosion, general corrosion refers to the relatively uniform reduction of material thickness. The breakdown of protective coating systems on structure surfaces often leads to this form of corrosion. Uniform attack can be prevented or reduced by proper material selection, including metallic or organic coatings and the modification of the medium (pH, temperature, addition of inhibitors, etc) [22]. It is also relatively easy to measure, predict and design against this type of corrosion damage. For example, it can be easily monitored using simple methods such as non-destructive thickness measurements.
- Crevice corrosion – It is a type of corrosion occurring at narrow openings or spaces, i.e. crevices. The crevices can be formed between two metal surfaces or between metals and nonmetal surfaces. Stagnant solution plays an important role in setting up highly corrosive micro-environments inside such crevices. Crevice corrosion is encountered particularly in metals and alloys which owe their resistance to the stability of a passive film, since these films are unstable in the presence of high concentrations of Cl^- and H^+ ions. Crevice corrosion geometries, such as the lap joints on aircraft fuselages, represent classic examples of "hidden" corrosions.
- Stress corrosion cracking (SCC) – It is a form of localized damage that refers to cracking under the combined influence of tensile stress and a corrosive environment. Stresses that can contribute to SCC include the applied, residual and thermal varieties, and also those generated by the build-up of corrosion products. SCC frequently occurs in media that are little or non-aggressive towards the metal or alloy in the absence of tensile loading (e.g. austenitic

stainless steels in high temperature water and steam). The associated weight losses are generally very small and even insignificant compared to the extent of the overall damage incurred[23]. This form of corrosion is of great practical importance and represents a permanent risk in numerous industrial installations, in terms of both the economic consequences and the safety considerations involved (personnel, equipment reliability, and respect of the environment). It is generally considered to be the most complex of all corrosion types.

- Intergranular corrosion – It refers to preferential (localized) corrosion along the grain boundaries, due either to the presence of impurities in the boundaries, or to the local enrichment or depletion of one or more alloying elements. The grain boundaries can undergo marked localized attack while the rest of the material remains unaffected. The alloy disintegrates and loses its mechanical properties. This selective disintegration may lead to the dislodgement of grains. It is difficult to detect intergranular corrosion in its early stages, since the overall loss of thickness remains minimal. Coupon exposures and microscopic examination of surfaces/metallographic cross sections are used to determine intergranular corrosions[24].
- Galvanic corrosion – It results from contact between two different metals or alloys in a conducting corrosive environment. When two or more different metals or alloys come into contact in the presence of an electrolyte, a galvanic couple is established as different metals have different electrode potentials[25]. It is this potential difference that is the driving force for galvanic current flow. The electrolyte provides a means for ion migration whereby metallic ions can move from the anode to the cathode[26]. The less noble material in the galvanic couple becomes the anode and tends to undergo accelerated

corrosion, while the more noble material (acting as a cathode) tends to experience reduced corrosion effects.

- Pitting corrosion – It is insidious and the attack is in the form of highly localized holes that can penetrate inwards extremely rapidly, while the rest of the surface remains intact. More detailed discussions on pitting corrosion of steel is provided below since the testing environment of the optical fiber corrosion sensor dedicated that pitting corrosion is the dominate type of corrosion observed by the optical fiber sensor.

2.1.1. Pitting corrosion

Pitting corrosion is a localized form of corrosion by which cavities or holes are produced in the material. It is considered much more dangerous than uniform corrosion. It forms on passive metals and alloys when the ultra-thin passive film (oxide film) is chemically or mechanically damaged and does not re-passivate immediately. The resulting pits become either wide and shallow or narrow and deep which can rapidly perforate the wall thickness of a metal. It occurs more readily in a stagnant environment and the rate of pitting is affected by the aggressiveness of the corrodent. The rate of penetration may be 10 to 100 times of that by general corrosion. It occurs much faster in areas where microstructural changes have occurred due to welding operation[27]. Apart from the localized loss of thickness, corrosion pits can also be harmful by acting as stress risers. Fatigue and stress corrosion cracking may initiate at the base of corrosion pits. One pit in a large system can be sufficient to produce the catastrophic failure of the entire system.

The different stages of pitting corrosion are

- ❖ Pit initiation - An initial pit may form on the surface covered by a passive oxide film as a result of the following:

- Mechanical damage of the passive film caused by scratches. Anodic reaction starts on the metal surface exposed to the electrolyte and the passivated surrounding surface act as cathode.
- Localized stresses in form of dislocations emerging on the surface may become anodes and initiate pits.
- Non-homogenous environment may dissolve the passive film at certain locations where the initial pits form.

❖ Pit growth - Pits grow by autocatalytic mechanism in the presence of chloride ions.

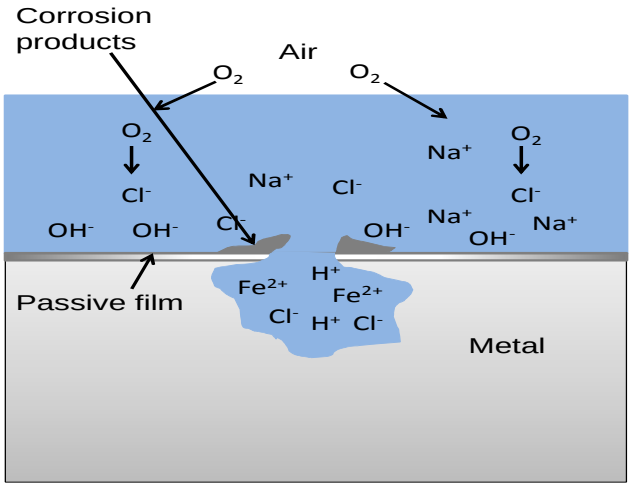

Figure 2.2: Pitting corrosion of steel.

Figure 2.2 shows the formation process of a corrosion pit. The driving power for pitting corrosion is the lack of oxygen around a small area. The presence of chlorides significantly aggravates the conditions for pit formation and growth through an autocatalytic process. Since the pits become loaded with positive metal ions through anodic dissociation, the Cl^- ions become concentrated in the pit for charge neutrality. This encourages the reaction of positive metal ions with water to form a hydroxide corrosion product and H^+ ions. As a result, the

pits become weakly acidic, which in turn further accelerates the process. The anodic reaction inside the pit can be described as:

$Fe = Fe^{2+} + 2e^-$ (dissolution of iron)

The electrons flow to the passivated surface acting as cathode where they are discharged in the cathodic reaction.

$1/2O_2 + H_2O + 2e^- = 2(OH^-)$

The electrolyte in the pit gains positive electrical charge as a result of the above reactions. In contrast, the electrolyte surrounding the pit becomes negatively charged. The positively charged pit then starts to attract negative ions of chlorine (Cl^-) and thus increase the acidity of the electrolyte according to the reaction:

$FeCl_2 + 2H_2O = Fe(OH)_2 + 2HCl$

The PH of the electrolyte inside the pit decreases as a result of the increase in acidity which causes further acceleration of the corrosion process. A large surface area ratio between the anode and cathode areas also favors corrosion rate increase.

2.2 Optical fibers

An optical fiber is a glass or plastic fiber that carries light in the fiber core. It allows light to be transmitted from one end to the other end with little attenuations. Figure 2.3a shows the basic structure of a fiber. It consists of three parts; the core, the cladding and the coating. The fiber core has a higher refractive index and is surrounded by an optical material that has a slightly lower refractive index, i.e. the fiber cladding, which traps the light inside the core by total internal reflection. The core and cladding are usually made of ultra-pure glass while some are all plastic or a glass core and plastic cladding[28]. The fiber is then coated with a protective coating that protects it from moisture and other physical damages. Figure 2.3b shows the propagation of light in the fiber. The acceptance angle of the fiber, i.e. the numerical aperture,

determines which light will be guided down the fiber. Any light entering the fiber at less than this angle will meet the cladding at an angle greater than the critical angle, resulting in the total internal reflection (TIR), i.e. all the energy in the ray of light is reflected back into the core and none escapes into the cladding. The ray then crosses to the other side of the core and, because the fiber is more or less straight, the ray will meet the cladding on the other side at an angle which again causes TIR. The ray is then reflected back across the core again and the same thing happens. In this way the light zigzags its way along the fiber and is transmitted to the end of the fiber with very low attenuation.

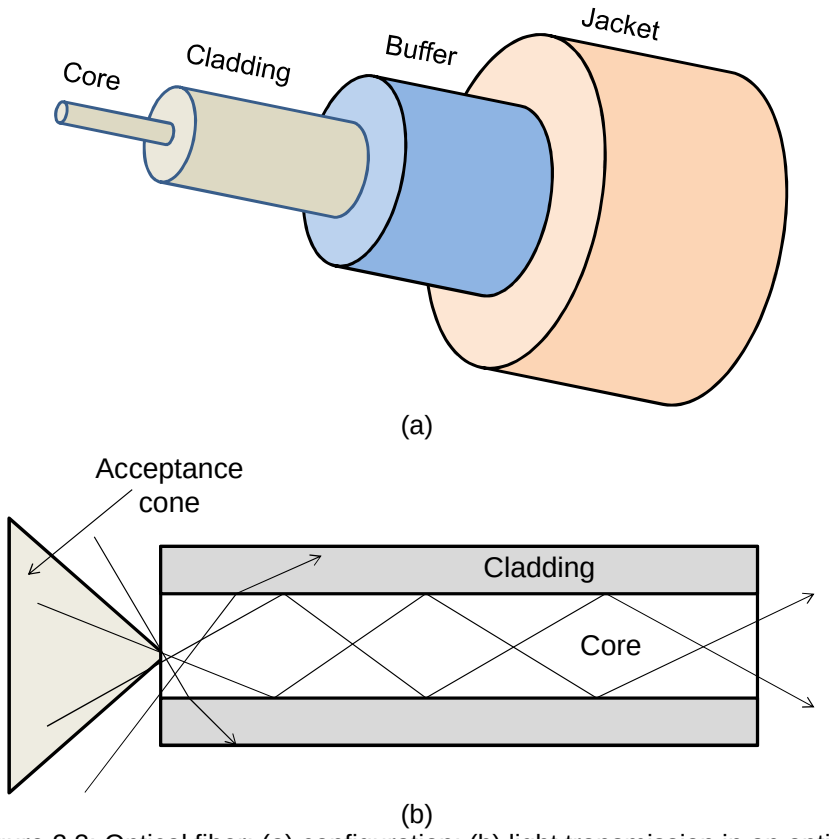

Figure 2.3: Optical fiber; (a) configuration; (b) light transmission in an optical fiber.

The geometry and composition of the fiber determine the discrete set of electromagnetic fields that can propagate in the fiber. These fields are called the fiber's modes. There are two broad classifications of the light modes: radiation modes and guided modes.

Radiation modes carry energy out of the core and the energy is quickly dissipated. Guided modes are confined to the core and propagate along the length of the fiber, transporting information and power. If the fiber core is large enough, it can support many simultaneous guided modes. Each guided mode has its own distinct velocity. Based on the number of fiber modes that can propagate in the fiber core, optical fibers can be classified as the following two types:

- Single-mode fiber (SMF) – with a SMF has a small core diameter and can only propagate one mode of light. A typical single-mode fiber has a core diameter between 8 and 10 µm and a cladding diameter of 125 µm. The small core and the single light-wave virtually eliminate any distortion that could result from overlapping light pulses, providing the least signal attenuation and the interference. The beam profile of the light propagating in a SMF can be approximated as being Gaussian.
- Multi-mode fiber (MMF) – A MMF has a much larger core diameter than that of SMF and thus allow the co-propagation of multiple guided modes. The number of modes propagating in a MMF increases with the core size and the numerical aperture. MMFs generally have core diameters of 50 µm, 62.5 µm, or 100 µm. The cladding diameter of MMF is 125 µm, the same as that of a SMF.

Figure 2.4 illustrates light transmission in single-mode and multi-mode fibers. In MMFs, the light rays enter the fiber at a range of angles, and the rays at different angles can all stably travel down the length of the fiber as long as they hit the core-cladding interface at an angle larger than the critical angle. For SMF, all rays in the optical fiber propagate in the same fashion.

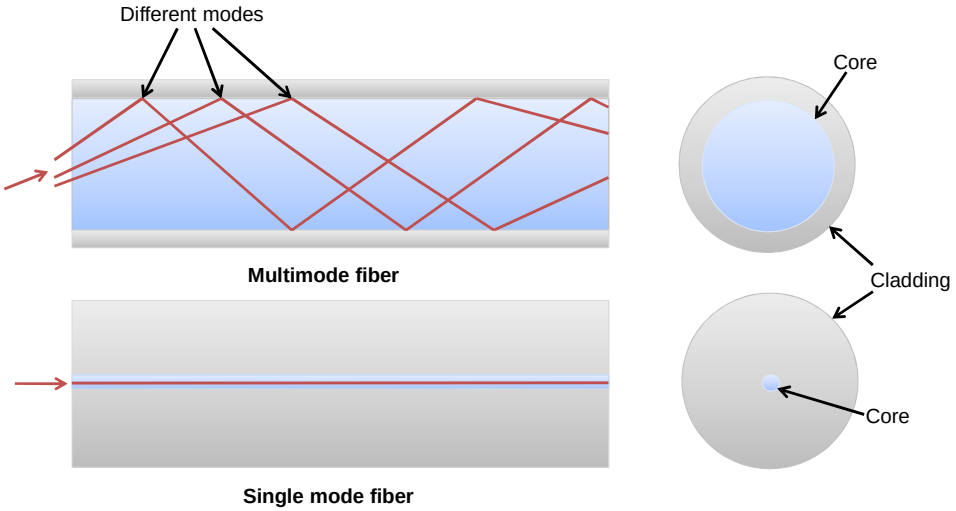

Figure 2.4: Comparison of SMF and MMF.

2.2.1. Optical fiber sensors

An optical fiber sensor is defined as a sensor that measures a physical quantity based on its modulation on the intensity, spectrum, phase, or polarization of the light traveling in an optical fiber. Optical fibers sensors have been developed to measure strain, temperature, pressure, refractive index, distance and other quantities [29] [30] [31] [32]. Their diversified nature is mainly due to the set of advantages that they offer, including:

- Compact size and multifunctional,
- Excellent resolution and range,
- Remote accessible,
- Multiplexed in parallel or in series,
- Resistant to harsh environment,
- Immunity to electromagnetic interference,
- Modest cost per channel.

An optical fiber sensing system is basically composed of a light source, optical fibers, a sensing element and a detector. The sensing element modulates a particular parameter of the optical light (intensity, wavelength, polarization, phase, etc.) which cause a change in the

characteristics of the optical signal received at the detector. Based on the measurement schemes, optical fiber sensors can be classified into two broad categories: wavelength-based and intensity-based sensors.

Wavelength-based sensors measure the physical parameter based on its influence on the wavelength of the light. In a wavelength-based measurement scheme, the sensitivity to any parameter is recorded as a change in the wavelength domain. A Long Period Fiber Grating (LPFG) based sensor is an example of a wavelength-based sensor. LPFGs are periodic perturbations in the effective refractive index of the optical fiber, which couples a part of light into the fiber cladding. As a result, the light travelling in the core displays a resonance loss at a particular wavelength when the light intensity is presented in the wavelength domain. Figure 2.5 shows a typical LPFG. The wavelength at which the coupling takes place is determined by the periodic perturbations as well as the effective refractive index[33]. Several physical changes in the region surrounding the LPFG, such as refractive index, temperature etc. can cause this wavelength to shift. Hence, LPFG serves as a very effective wavelength based sensor.

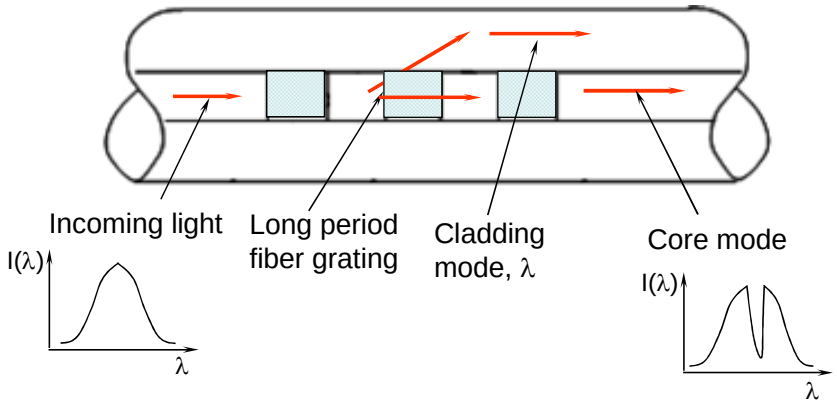

Figure 2.5: Long Period Fiber Grating (LPFG).

Intensity-based sensors measure a physical parameter based on its effect on the intensity of either the reflected or transmitted light. The corrosion sensor discussed herein is an example of an intensity-based sensor.

2.2.2. Optical components

The different types of optical components used in this thesis work are described as the following:

- Light source – A light source is a device that provides a stable source of electromagnetic energy at a given wavelength. An LED and a laser are two most common light sources for optical fiber sensors. LEDs are typically used for multimode fibers. On the other hand, lasers are used for single-mode fiber applications.
- Photo-detectors – A photo-detector contains a photodiode that convert electromagnetic energy into electric energy and produces a current output. When a photon is absorbed by the photodiode, it excites an electron, creating an electron-hole pair within the device. If the absorption occurs in the junction's depletion region, these carriers are swept from the junction by the built-in field of the depletion region. Thus holes move toward anode and the electrons toward the cathode, thereby producing a current proportional to the light intensity. The measure of this photocurrent provides a measurement of the optical power incident upon the detector. Currently, photo-detectors using silicon (for multimode applications), germanium (for single-mode and multimode applications), and InGas (for single-mode and multimode applications) technologies are available.
- Power meter – An optical power meter measures either the current or voltage generated by a photo-detector and provide a reading on the power of the incident light. A typical optical power meter device consists of a calibration circuit account for a detector's responsivity at the measurement wavelength.
- Coupler – A fiber optic coupler is an optical fiber device with a set of input fibers and a set of output fibers. Light from an input fiber is distributed to one or more output fibers. Fiber optic coupler specification includes the numbers of input and output ports,

insertion loss, and splitting ratio. Based on the number of input and output ports, couplers can be star or tee types. Star-type couplers have ‘N’ inputs and ‘N’ outputs (N×N). Tee-type couplers have one input and ‘N’ outputs (1×N). Insertion loss is the attenuation caused by the coupler. The splitting ratio, also referred as the coupling ratio, is the distribution of optical power among the output fibers of a coupler.

CHAPTER 3

OPERATING PRINCIPLE OF OPTICAL FIBER CORROSION SENSOR

In this chapter, the fundamental working principles of the optical fiber corrosion sensor and the laser reflectance sensor are discussed.

3.1 Principle of operation of optical fiber corrosion sensor

A diagram of the optical fiber corrosion sensor is shown in Figure 3.1a. It consists of two subsystems: an optical fiber reflectivity sensing system and a tube/film subassembly. The optical fiber reflectivity sensing system includes a laser as the light source, a sensor probe that delivers the laser light to the film surface using a signal model fiber (SMF) and collects the reflected light using a multimode fiber (MMF) [21], and a power meter that measures the power of the reflected light. The tube/film subassembly is manufactured by laser welding a stainless tube to a sacrificial metallic film. The sensor probe and the tube/film subassembly are packaged into a sensor head. Figure 3.1b shows the enlarged view of the sensor head. The side of the sacrificial film that is enclosed by the sensor head, i.e. the inner surface, is finely polished and isolated from the environment while the other surface of the film, i.e. the outer surface, is exposed to the corrosive environment. Corrosions will be initiated at the outer surface first and grow deeper into the sacrificial film as the exposure time increases. The reflectivity of the inner surface reduces once the corrosion pits reach the polished side of the film, resulting in a decrease in the reflected light that is collected by the sensor probe. The sensor only detects the corrosion when the corrosion is severe enough to penetrate through the thickness of the sacrificial film. By choosing the proper thickness of the sacrificial film, corrosions of various degrees can be detected.

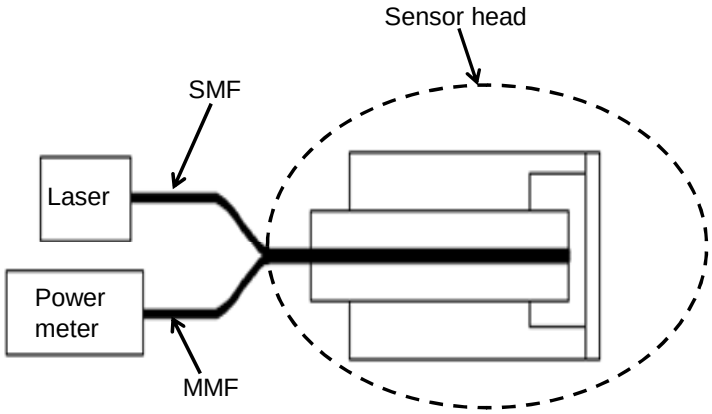

(a)

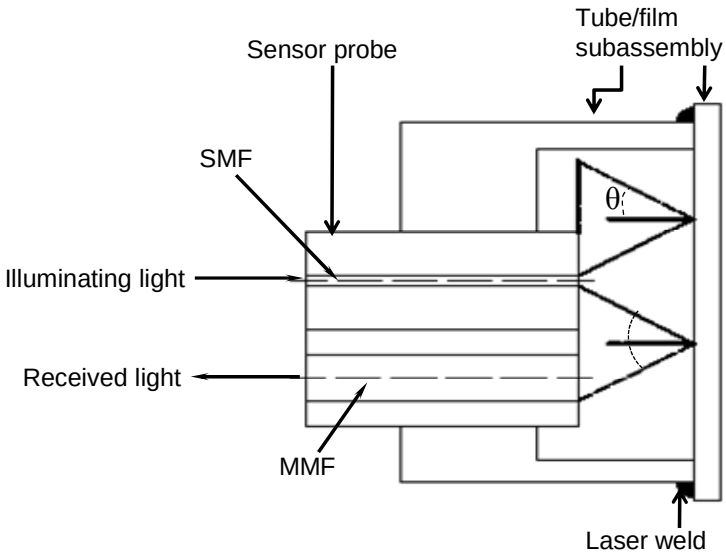

(b)

Figure 3.1: Corrosion sensor configuration; (a) optical fiber corrosion detection system; (b) enlarged view of the sensor head.

3.2 Principle of operation of sensor probe

The principle of operation of the optical fiber sensor probe is briefly described here and its detailed discussion was given by Huang and Tata [34] . The sensor probe consists of two optical fibers, a SMF and a MMF. The target (sacrificial metallic film) is placed in front of the sensor probe. The light exiting the SMF gets reflected by the target and a part of this reflected

light is collected by the MMF. The intensity profile of the light travelling in the SMF is approximated as having a Gaussian profile (see Figure 3.2) and is assumed to maintain this profile after it exits the SMF. Exiting from the SMF, the light diverges with a cone shaped radiation pattern at an angle θ that increases in size, which cause the light intensity to reduce. As a result, the intensity of the light collected by the MMF changes with the target position. In order to couple the reflected light into the receiving fiber, the distance between the target and the sensor probe has to be sufficiently large so that the reflected light pattern intersects with the core of the MMF. A typical power-position relationship, obtained using a mirror as the target, is shown in Figure 3.3. The effect of change in the target distance on the sensor output can be explained from the location of the receiving fiber (MMF) in the reflected radiation pattern. For a small target distance, the receiving fiber is located outside of the radiation pattern, resulting in a 'dead zone' in the power-position profile (up to distance 0.2 mm in Figure 3.3). As the target distance increases, the sensor output increases steadily due to enlarged radiation pattern, which is equivalent to moving the MMF toward the center of the radiation pattern. The sensor output reaches its peak value when the core of the MMF coincides with the boundary of the mode field. Further increase in distance results in a decrease in the sensor output. This is because the intensity of the reflected light decreases as the target distance increase, while the light collecting area remains constant. In case the target surface is not mirror-smooth, the surface roughness of the target surface will broaden the reflected light pattern and thus decrease the power of the collected light. Therefore, the sensor probe can also serve as a surface roughness sensor [35] .

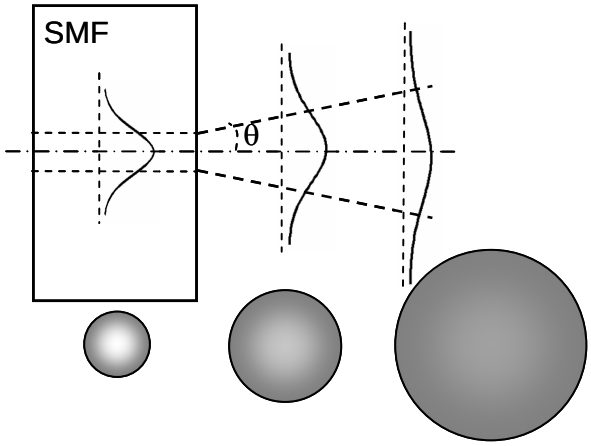

Figure 3.2: Intensity profile of the illuminating light.

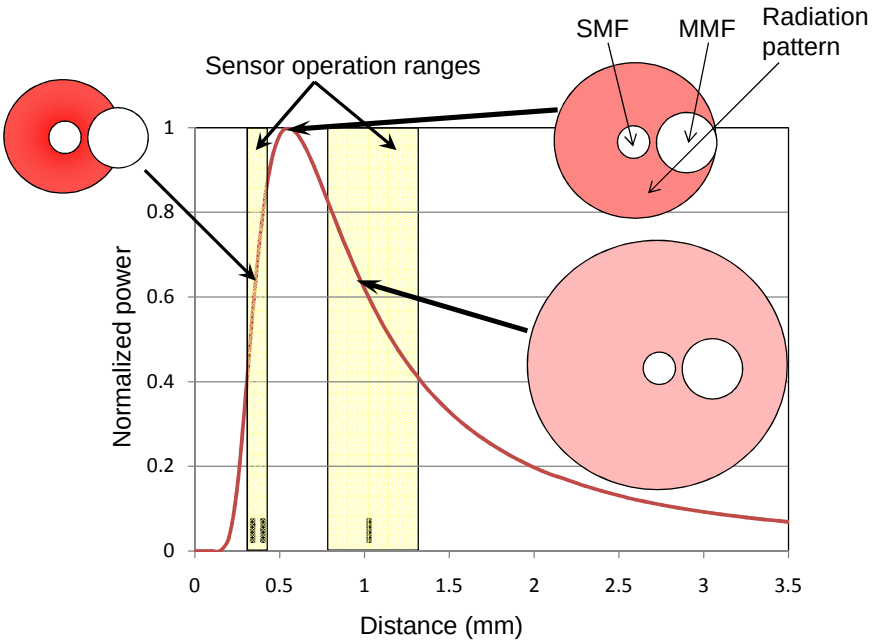

Figure 3.3: Power-position relationship of a laser reflectance sensor probe.

Based on the power-position curve shown in Figure 3.3, the distance between the sensor probe and the sacrificial metallic film can be adjusted precisely during the corrosion sensor assembly. For the corrosion sensors, the output power fluctuations should be small and the inspection area on the sacrificial film should be as large as possible. The two shaded areas are potential sensor operation range. Sensor range II is sensitive to distance variations because of the steep slope. Small distance perturbations, such as those caused by vibration, could

cause fluctuation in the output power of the sensor operating in this sensor range. In contrast, sensor range I has a less steep slope. Therefore, the sensors operating at this range is less sensitive to distance distribution. The size of the inspection area is also important for the design of the corrosion sensor. The corrosion sensor can only detect the corrosions when they are located within the inspection area. Since pitting corrosions occur at discrete locations, a large inspection area will likely to detect the corrosion pits as soon as they penetrate through the sacrificial film. For a small inspection area, however, the sensor has to wait until the corrosion progresses to the inspection area since the chance of having a corrosion pit in the inspection area is small. Because the inspection area is controlled by the distance between the sensor probe and the sacrificial film, the relationship between the distance and the inspection area is analyzed in the next section.

3.3 Analysis of inspection area

The area under the inspection of the sensor probe is determined by the distance between the source light and the sacrificial film. The relationship between the sensor/film distance and the inspection area needs to be established in order to select the optimized sensor/film. Figure 3.4 shows the sensor configuration at different views. The nomenclature used in the diagram is listed and summarized in table 3.1.

Table 3.1 Nomenclature and its definitions

Nomenclature	Definition	Value
D_F	Distance between the centers of light source (SMF) and the MMF	125 µm
r_M	Radius of the MMF core	25 µm
d_f	Distance between the centers of light source and the projected area of the MMF on the sacrificial film	62.5 µm
NA	Numerical aperture of the SMF	0.11

After exiting the SMF, the illumination light begins to diverge with an angle θ which can be calculated from the numerical aperture (NA) of the SMF as

$$\theta = \sin^{-1}(NA). \quad (3.1)$$

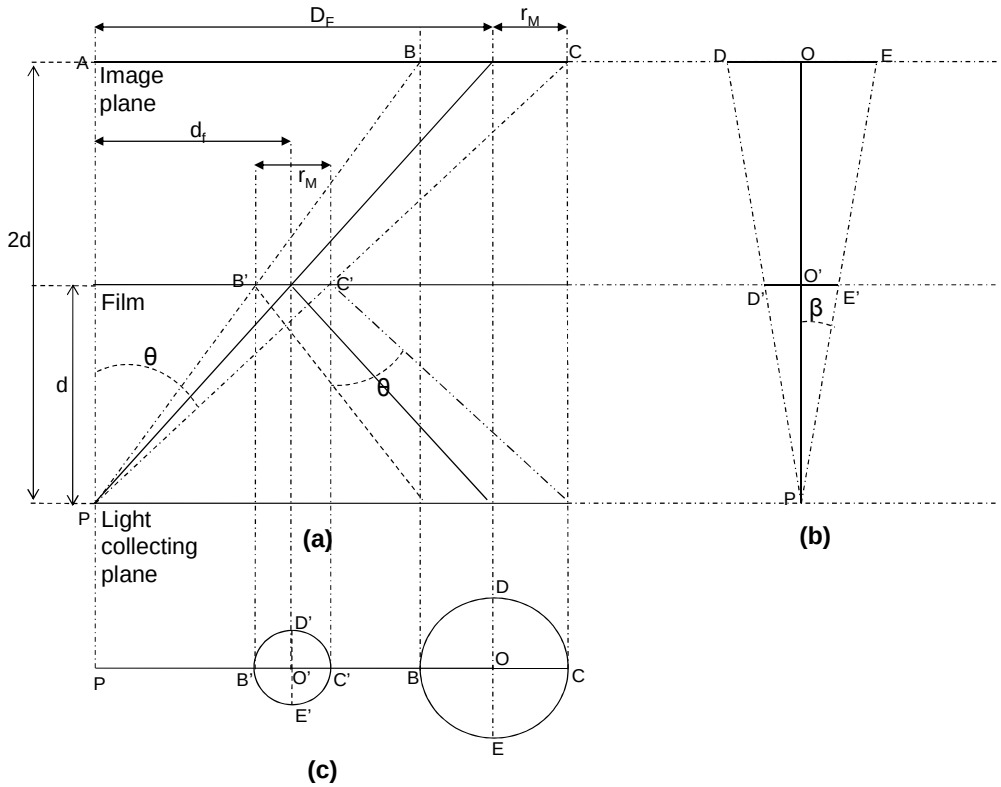

Figure 3.4: Sensor diagram; (a) top view; (b) side view; and (c) front view.

The reflected light pattern at the light collecting plane is the same as a virtual light pattern at an image plane behind the sacrificial film. The core area of the MMF (area BCDE) is the light collecting area at the light collecting plane. The lights incident on the area B'C'D'E' of the sacrificial film are reflected toward area BCDE and thus are collected by the MMF.

As shown in Figure 3.4 (a), the triangles PB'C' and PBC are similar as their corresponding (matching) angles are congruent (equal) and the ratios of their corresponding sides are in proportion. Therefore:

$$B'C' = (BC \times PC')/PC. \quad (3.2)$$

Substituting $BC = 2r_M$ and $PC'/PC = ½$ into equation 3.2, we have

$$B'C' = r_M. \quad (3.3)$$

Similarly, Figure 3.4(b) gives

$$D'E' = r_M. \quad (3.4)$$

Therefore, the projection of the MMF core of radius r_M from the image plane (light collecting plane) on the sacrificial film is a circle of diameter r_M.

Since the light source diverges in a cone-shaped pattern with an angle θ, the radius of the light pattern impinged on the sacrificial film increases with the distance d. The intersection of the light pattern and the projected MMF circle is shown in Figure 3.5. The overlapping area between the two circles i.e. the shaded area in Figure 3.5, is the area under inspection.

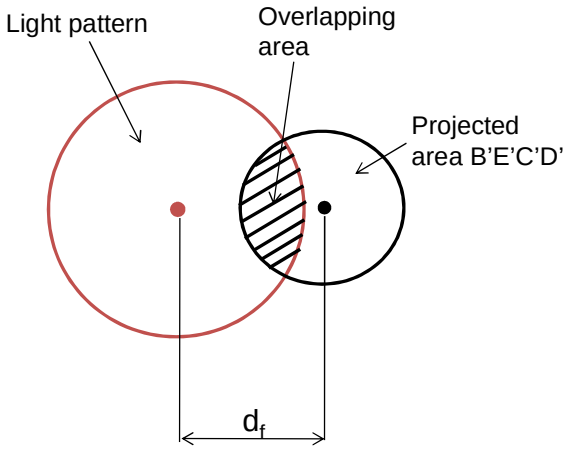

Figure 3.5: Intersection of light pattern with the projected MMF circle.

The two circles, i.e. the illumination light pattern and the projected MMF circle, can be represented as

$$x^2 + y^2 = R^2. \tag{3.5}$$

and

$$(x - d_f)^2 + y^2 = (r_M/2)^2. \tag{3.6}$$

The intersecting area is calculated using the formula [36]:

$$A_1 = \left(\frac{r_M}{2}\right)^2 COS^{-1}\left(\frac{d_f{}^2 + \left(\frac{r_M}{2}\right)^2 - R^2}{2d_f\left(\frac{r_M}{2}\right)}\right) + R^2 COS^{-1}\left(\frac{d_f{}^2 + R^2 - \left(\frac{r_M}{2}\right)}{2d_f R}\right) - \frac{1}{2}\sqrt{\left(-d_f + \left(\frac{r_M}{2}\right) + R\right)\left(d_f + \left(\frac{r_M}{2}\right) - R\right)\left(d_f - \left(\frac{r_M}{2}\right) + R\right)\left(d_f + \left(\frac{r_M}{2}\right) + R\right)} \tag{3.7}$$

In equation 3.7 the radius *R* of the source pattern varies with sensor/film distance *d* as

$$R(d) = (r_0 + d \tan\theta)\sqrt{(-\ln X)} \tag{3.8}$$

where r_0 is the mode field radius of the SMF core, and X = 2% is the minimum power percentage at which the sensor output starts to increase after the dead zone on the power-position curve shown in Figure 3.3. Figure 3.6 shows the variation of the inspection area with the sensor/film distance. At the beginning, the source doesn't intersect with the projected MMF circle. As the distance *d* increases, the size of the light pattern increases. At a distance of 0.2 mm, it begins to intersect with the projected MMF circle, resulting in an increase in the area being inspected. As the distance increases further, the entire projected MMF circle is covered by the light pattern, which means the area being inspected on the film reaches a maximum value. Any further increase in distance dos not increases the inspection area but reduces the power of the collected light since the intensity of the illumination light reduces with the distance. Figure 3.6 also shows the output power-position profile of the optical fiber reflectance sensor. Sensor operation range I inspect a larger area on the film compared to sensor range II. Thus the distance between the sensor probe and the sacrificial film is selected accordingly so that the corrosion sensor operates in sensor range I.

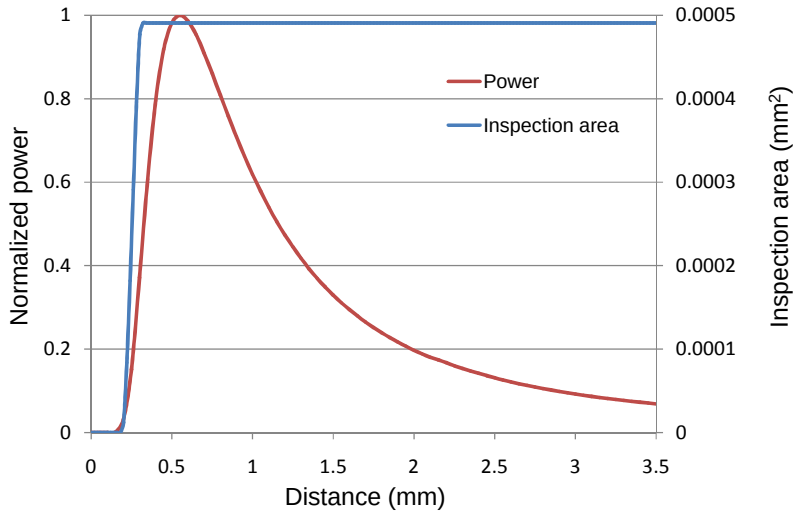

Figure 3.6: Variation of inspection area and power with sensor/film distance.

CHAPTER 4

IMPLEMENTATION AND CHARACTERIZATION OF OPTICAL FIBER CORROSION SENSOR

The fabrication and packaging of the corrosion sensor, sensor multiplexing, experiment procedure, and the discussion and analysis of the experimental results are presented in this chapter.

4.1 Sensor probe fabrication and validation

4.1.1. Sensor probe fabrication

Figure 4.1 shows different stages of sensor probe fabrication and preparations. The sensor probe was constructed by packaging one SMF and one MMF with a 50 µm core inside a stainless steel tube (1 inch in length, 0.0625 inch outer diameter and 0.03 inch inner diameter). The coatings of the SMF and MMF were stripped at their ends (not more than 1 inch) and were aligned properly inside the tube. An optical fiber epoxy (Thorlabs, F112) was then injected into the tube through a syringe and left to cure for 24 hours. Subsequently, the optical fibers were cleaved using a scriber. The sensor probe was then inserted into a polishing disk and polished in a circular “figure 8” pattern on aluminum oxide polishing films, following the same procedures as that for fiber connector preparation (Thorlabs, connector polishing guide), in the order of grit sizes 5 µm, 3 µm, 1 µm and 0.3 µm.

A microscopic image of a properly polished sensor probe is shown in Figure 4.2.

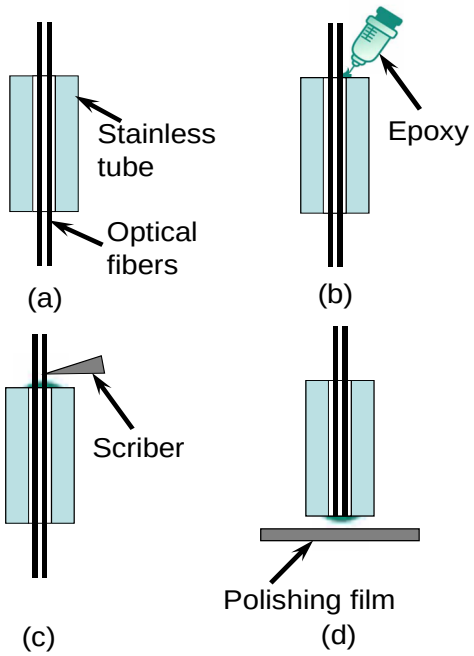

Figure 4.1: Sensor probe packaging; (a) fiber alignment; (b) epoxy injection; (c) fiber cleaving; (d) sensor probe polishing.

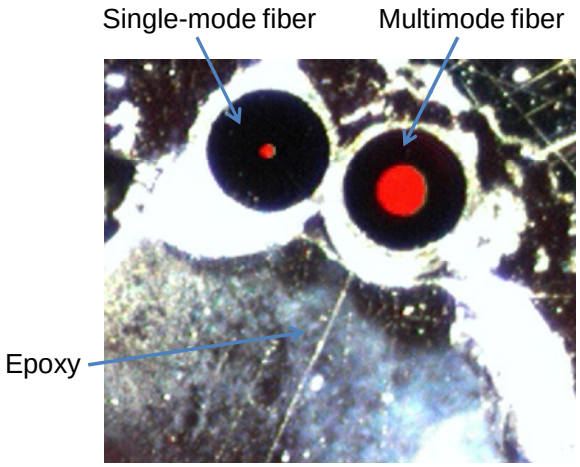

Figure 4.2: Microscopic image of a polished sensor probe.

4.1.2. Sensor probe validation

The function of the sensor probe was validated using the bench top test unit shown in Figure 4.3. The coordinate system is defined based on the orientation of the sensor probe. The Z-axis is aligned with the axial direction of the sensor probe, the Y-axis represents the horizontal direction and the X-axis represents the vertical direction. The polished sensor probe

was placed on a stationary platform. A mirror, serving as the target, was mounted on a motorized translation stage in front of the sensor probe with its surface perpendicular to the axis of the sensor probe. The SMF of the sensor probe was connected to a 1550 nm, 19.4 mW distributed feedback (DFB) laser source (Amonics ADFB-1550-10). The MMF was connected to an optical power detector (Newport 818-IR) which in turn was connected to an optical power meter (Newport 1815-C). The sensor output was monitored using a computer-based data acquisition system (Data translation DT 9812) and the mirror position was traversed by the motorized translation stage (Newport 561D). The mirror positions as well as the power meter reading at each position were recorded. A smooth power-position curve similar to Figure 3.3 indicates that the sensor probe is properly assembled and polished.

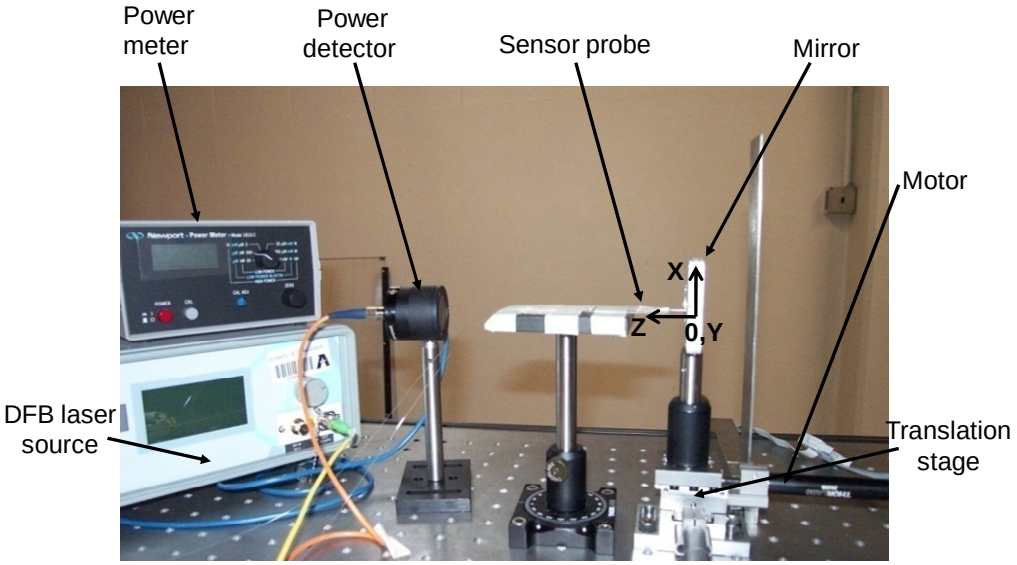

Figure 4.3: Bench top characterization of sensor probe.

4.2 Corrosion sensor packing

Cold rolled SAE 1010 steel film with a thickness of 127 µm (0.005 inches) was selected as the sacrificial material. One side of the steel film was polished on silicon carbide polishing films with different grit sizes in the order of 220, 400, 600 and 1500 to achieve a mirror-like surface. The polished films were then profiled by the sensor probe, following the procedure

discussed in section 4.1.2. The power-position relationships for the four polished films are plotted in Figure 4.4a. Compared to that obtained using a mirror; the sensor outputs for the polished films were about 40% lower. The smoothness of the curves indicated that the films were polished uniformly. The thickness of the polished films was measured to be 0.0043 inch using a depth gauge (Import, dial gauge comparator stand). The polished side of the steel films was then laser welded to stainless steel tubes having an outer diameter of 6.35 mm (0.25 inch), an inner diameter of 3.86 mm (0.152 inch) and is 12.7 mm (0.5 inch) in length to form the tube/film subassembly. The stainless steel tube also serves as the housing for the sensor head. The tube/film subassembly and the sensor probe were assembled by placing the tube/film subassembly on a three-axis motorized translational stage and the sensor probe on a stationary platform. Care was taken to align the sensor probe properly so it was perpendicular to the sacrificial film and was placed at the center of the tube. During assembly, the power-position relationship was again obtained by traversing the sensor probe and measuring the power of the reflected light (see Figure 4.4b). The sensor outputs before and after the laser welding were similar, indicating that the laser welding did not change the surface characteristics of the films. Based on the power-position relationship, the assembly positions of the sensor probes were chosen to be between motor positions 2 mm to 4 mm, i.e. sensor operation range I. The sensor output was monitored over time at the predetermined position chosen for each of the sensors. A program was written in VC++ to record and store the obtained data. As shown in Figure 4.4c, sensor outputs of the four sensors remained stable over a period of 30 minutes.

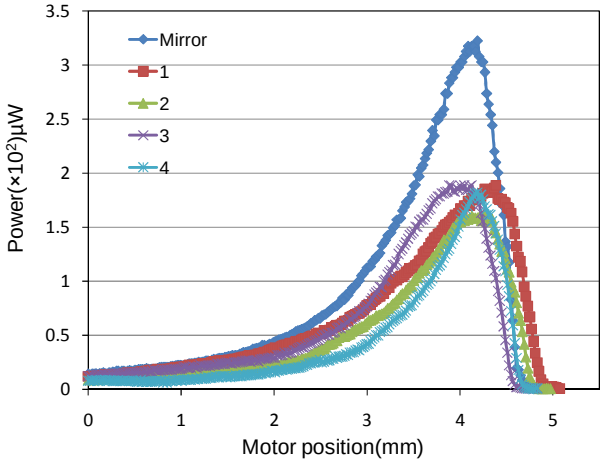

(a)

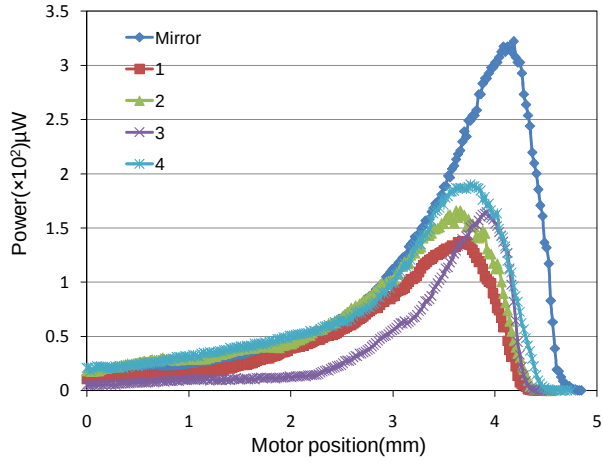

(b)

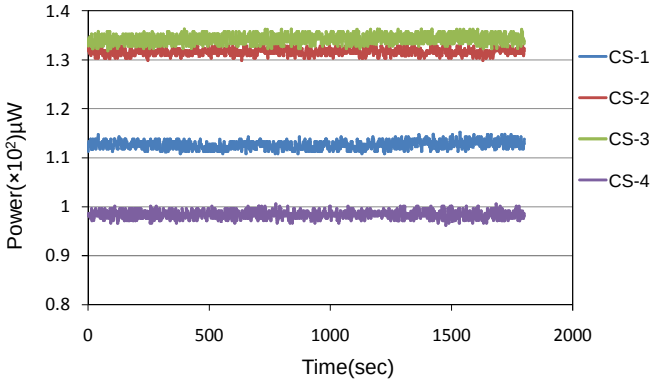

(c)

Figure 4.4: Power-position profile of polished films; (a) Before welding; (b) After welding; and (c) Stable sensor output over time.

Once the sensor probe was positioned properly in the tube/film subassembly at a predetermined position, it was glued to the tube/film subassembly using a water proof epoxy (Loctite epoxy gel 1106702). To further protect the welding and the epoxy from the environment, the packaged sensors were coated with 4 layers of rust control paint (ACE rust stop, primer and indoor/outdoor). The central portion of the sacrificial film was carefully covered with a masking tape before the application of the rust control paint. After the rust control paint was fully dried, the masking tape was removed to expose the film surface. The output of each sensor was checked again after the removal of the masking tape to ensure that no damage was done to the sacrificial film during packaging or rust control application. The front and bottom view of a packaged sensor is shown in Figure 4.5. The front view shows the general overview of the packaged corrosion sensor and the bottom view shows the area of the film that is not covered by the rust control coating, i.e. the exposed area. This area was polished with a rough silicon carbide polishing film of grit size 220 to remove the passive protective film of the steel surface and thus expedites the corrosion process.

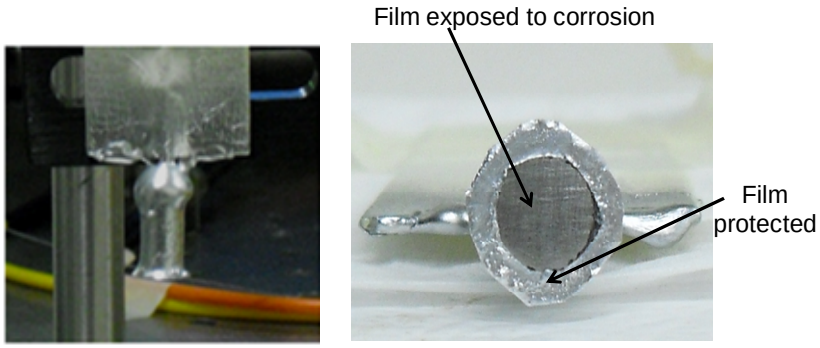

Figure 4.5: Packaged sensor; (a) front view; and (b) bottom view.

4.3 Multiplexing of corrosion sensors

Multiplexing refers to a process where the outputs of multiple sensor channels are combined for signal transmission over a common transmission path. In order to monitor multiple sensors at one time, the packaged sensors were multiplexed using optical fiber couplers. As

shown in Figure 4.6, a 60 mW Erbium-doped Fiber Amplifier (EDFA) supplies the laser light to a 1×4 single mode coupler (SMC, P/N-SSSCA1X415510), which divides the input into four outputs. Each output was connected to the SMF of the corrosion sensors using connector sleeves. The outputs of the four sensors were connected to a 4×1 multi-mode coupler (MMC, AC Photonics-MP15AV0104S2200). The MMC combines the four sensor outputs and sends one single signal to the power meter. The power distribution and the power output of each sensor are tabulated in Table 4.1. P4x represents the power output of system when only sensor x was connected while the other three sensors were disconnected. When all four sensors were connected, the output of the multiplexing assembly P4 was a summation of P4x. The sensor output values of table 4.1 gives an indication about which corrosion sensor has gone bad (corroded), when there is a decrease in the cumulative power output value. The advantage is that a particular corroded sensor can be identified from the multiplexed output without disassembling and checking the outputs of each corrosion sensor individually.

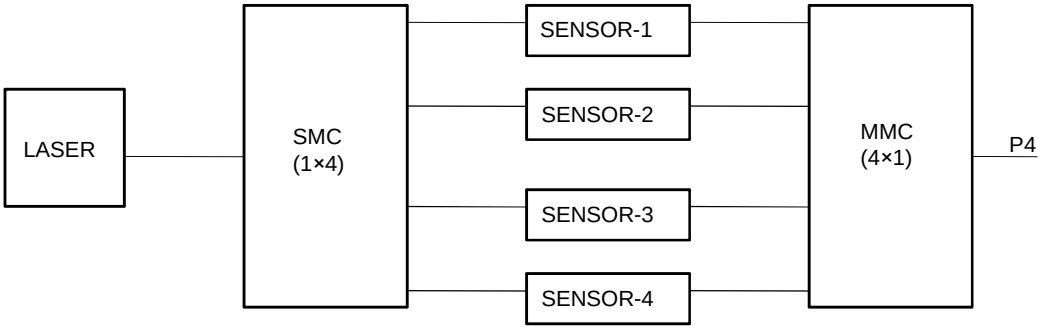

Figure 4.6: Multiplexing of multiple corrosion sensors.

Table 4.1 Initial power output readings of corrosion sensors

Laser output (mW)	P41 (µW)	P42 (µW)	P43 (µW)	P44 (µW)	P4 (µW)
47.1	6.75	7.8	6.2	9	29.75

4.4 Results and discussions

The performance of the optical fiber based corrosion sensor was validated in two steps. First, a steel disk with alternative corrosion bands was characterized using the laser reflectance sensor to confirm that corrosion reduces the sensor output. Second, the packaged corrosion sensors were immersed in saline solutions over time to detect the corrosion development in the sacrificial films.

4.4.1. Characterization of corroded steel disk

SAE-1018 steel disk was polished on silicon carbide polishing films with different grit sizes in the order of 220, 400, 600 and 1500 to achieve a mirror-like finish. The polished surface of the steel disk was applied with several bands of nail polish to mask out the regions that were not intended to be exposed to the environment. The masked disk was then submerged in 1%Nacl saline solution for three weeks and taken out once significant corrosions were developed in the regions that were not coated with nail polish. In order to remove any superficial corrosion development on the surface the corroded disk was polished with polishing films. An image of the corroded regions and non-corroded regions after polishing is shown in Figure 4.7. The difference in height between the corroded and non-corroded regions of the steel disk, measured using a depth gauge, was 0.038 mm (0.0015 inch), means that the loss of material at the corroded section was 0.038 mm.

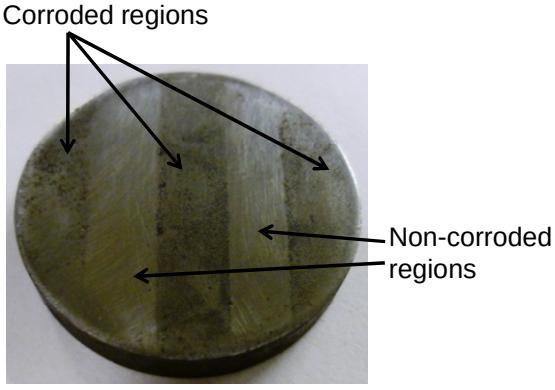

Figure 4.7: Corroded and non-corroded regions of the steel disk.

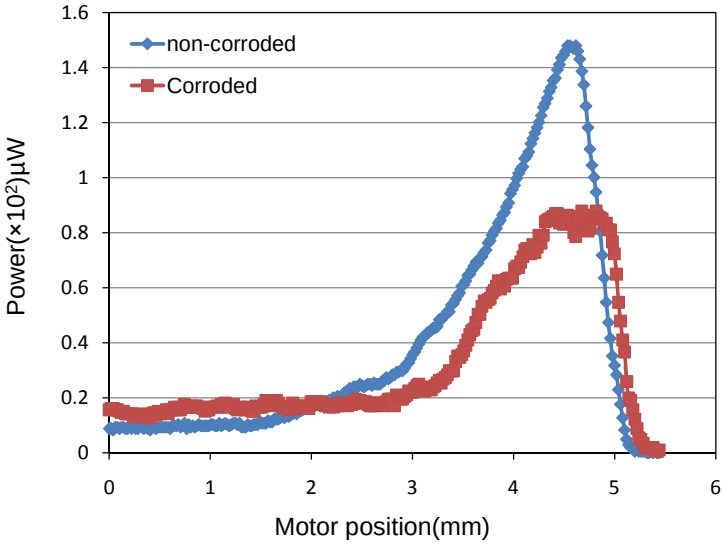

(a)

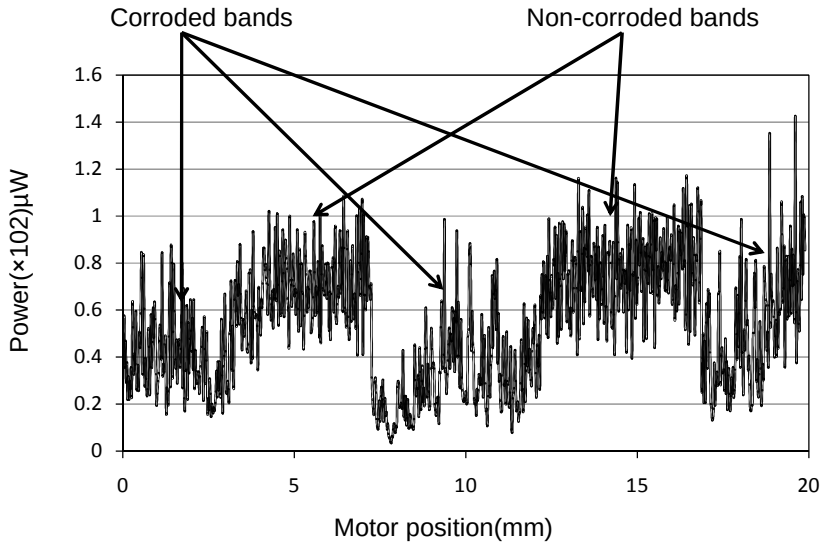

(b)

Figure 4.8: Sensor outputs at corroded and non-corroded region; (a) power-position relationship; (b) sensor outputs at a fixed distance between the sensor and the disk.

Following the same procedure discussed in section 4.1.2 (using the corroded disk as the target), the power-position relationship for the non-corroded and corroded regions were obtained and plotted in Figure 4.8a. The sensor output at the corroded region was about 30% lower than that for the non-corroded region. The sensor power output fluctuations were more for

the corroded profile than that for the non-corroded profile. Next, the distance between the sensor probe and the corroded disk was fixed at a motor position of 3.88 mm (Z-distance) and the variations in the sensor power output as the disk was traversed perpendicular to the alternating bands of corroded and non-corroded regions (Y-distance) were obtained (Figure 4.8b). The average intensity at the corroded region is around 60 µW while it is around 80 µW at the non-corroded region. Since the depth differences between these two regions are relatively small, the decrease in the sensor output at the corroded sections are mainly due to corrosion-induced surface roughness increases.

4.4.2. Characterization of corrosion sensors

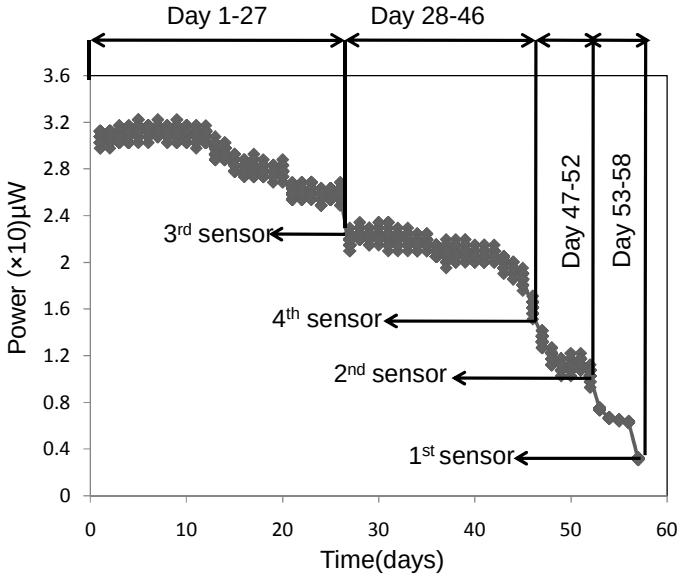

Figure 4.9: Cumulative power output over time.

To characterize the sensors' performance for corrosion detection, the packaged corrosion sensors were submerged in four solutions with saline concentrations of 1%, 2%, 3% and 4%. The cumulative sensor power output (P4) from the MMC was measured on a daily basis. The composition of the cumulative output of the corrosion sensors over 58 days is shown in Figure 4.9. The cumulative power was stable for the first 12 days and started to reduce gradually. On the 28th day, the cumulative power output reduced significantly, indicating that

one of the packaged corrosion sensors has detected corrosions. The decrease in the cumulative power output was 7 µW, indicating that one of the two sensors – senor-1 or sensor-3 has corroded, since their respective output is close to 7 µW (see table 4.1). Checking the output of both corrosion sensors (CS-1 and CS-3) revealed that the output of the sensor immersed in the 3% saline solution (CS-3) was reduced to zero. This sensor was then removed from the measurement system. After cutting the tube/film subassembly using a hand saw and measuring the thickness of the corroded film using a depth gauge, it was found that the thickness of the metallic film has reduced by 37%. The sensor probe of this corrosion sensor was also checked to determine whether the output reduction is due to a defective sensor or due to the corrosion of the sacrificial film. It was found out that the sensor probe was working properly. Therefore, the decrease in the output of the corrosion sensor was due to the corrosion of the sacrificial film. In addition, the inner surface of the sacrificial film was inspected under an optical microscope. The digital images of the sacrificial film before and after the corrosion process are shown in Figure 4.10. The corrosion pits are clearly visible on the inner surface. The corrosion pits appeared to be randomly distributed over the entire surface. Another observation is that the surface roughness of the polished surface appeared to have increased.

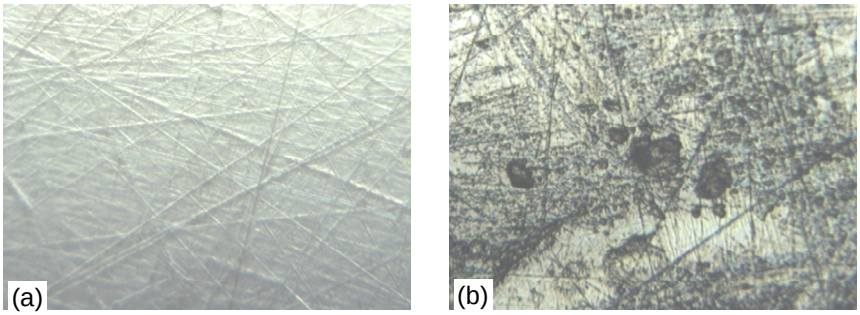

Figure 4.10: Images of the film; (a) before corrosion; and (b) after corrosion.

The cumulative power output of the remaining three corrosions sensors was again monitored on a daily basis. On the 47th day, the corrosion sensor immersed in 4% saline solution was giving a considerably low power output. Same procedure was followed in analyzing the corrosion sensor as discussed before. The percentage of change in the film thickness for

this sensor was found to be 60%. On the 53rd day, the corrosion sensor immersed in the 2% saline solution was removed and the reduction in thickness was 49%. At last, the corrosion sensor immersed in the 1% saline solution failed on the 58th day and subsequently measurement showed that the reduction in thickness for this sensor was 46%.

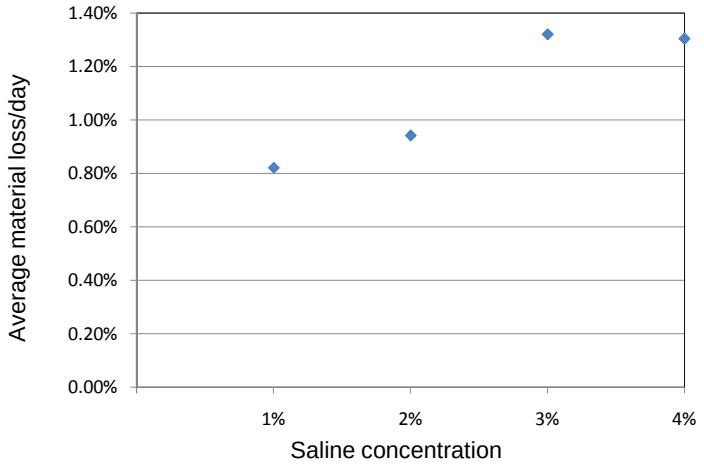

Figure 4.11: Material loss at different saline concentrations.

Figure 4.11 shows the average material loss per day for the sensors immersed in different saline concentrations. The percentage of reduction in material thickness increased almost linearly with the saline concentrate up to 3%. The material loss appeared to be saturated for saline concentration above 3%. The material loss at the time of detection varied from 37% for 3% saline concentration to 60% for 4% saline concentration while the material loss for 1% and 2% saline concentration are approximately the same, i.e. 46% and 49%. These variations in material loss at the time of detection may be explained by the sensor configuration. The illumination area of the sensor was relatively small as compared to the area of the film that was exposed to the environment. As shown in Figure 4.12 the corrosion pits are not uniformly distributed over the entire surface. Therefore, if the sensor probe was placed near a corrosion pit, the sensor may detect the corrosion pit earlier, *i.e.* at a smaller material loss. Otherwise, it has to wait until the corrosion pits spread to the illuminated region. To achieve a more consistent sensor performance in term of material losses, the film area that is exposed to the

environment should be reduced and matched well with the area under inspection by the sensor probe.

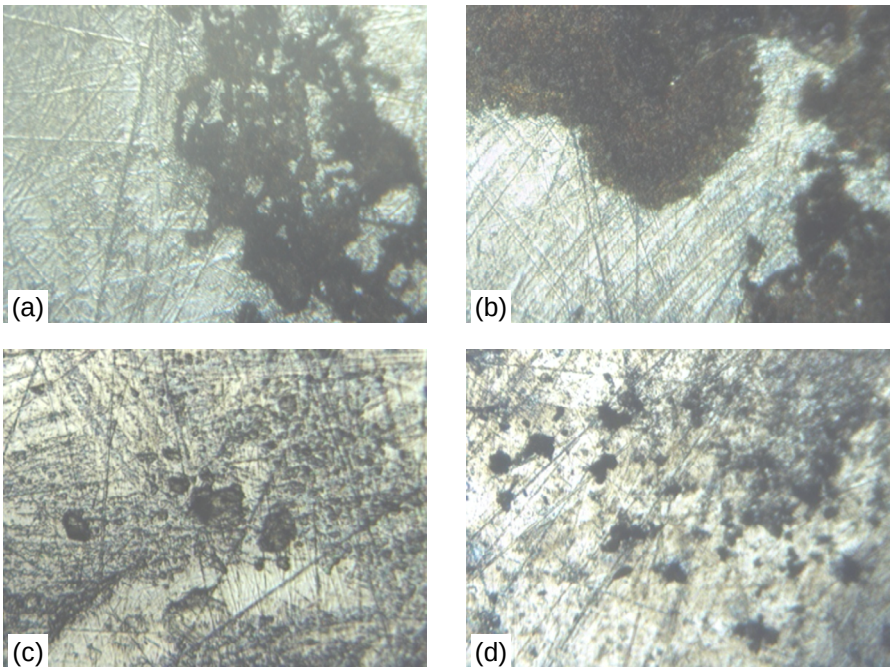

Figure 4.12: Images of the corroded surfaces of sacrificial films; (a~d) corroded surfaces of films immersed in 1%, 2%, 3% and 4% Nacl concentrations.

CHAPTER 5

IMPROVED OPTICAL FIBER CORROSION SENSOR

A few improvements on the optical fiber corrosion sensor were implemented and discussed in this chapter. The main aim of these improvements is to address the drawback of the corrosion sensors discussed in the previous chapter, i.e. inconsistent performance of the sensor in term of material losses.

5.1 Improved sensor fabrication and packing

As discussed in section 4.2, in order to achieve a more consistent sensor performance, the area that is exposed to the environment should be reduced. In addition, the sensor probe should be positioned properly so that the exposed area is located at the opposite side of the area under inspection. This requires a precise control of the position of the SMF inside the steel tube. One way to achieve precise position control is by reducing the inner diameter of the steel tube because reduced inside diameter limits the movement of the fibers during alignment and epoxy injection. By positioning the sensor probe at the center of the sensor housing and only exposing a small area at the center of the sacrificial film, the overlapping of the inspection area and the area exposing to the environment can be achieved, leading to most consistent sensor performance in terms of thickness loss at the time of inspection. The new steel tube selected for the improvement has an outer diameter of 0.9 mm (0.0358 inch) and an inner diameter of 0.70 mm (0.0278 inch). Three sensors were fabricated following the same procedure described above, except that a smaller mask was used to cover the center of the sacrificial film during the application of the rust-control coating. As shown in figure 5.1, the resulting exposed area is much smaller compared to that shown in figure 4.5. The packaged sensors were multiplexed as before and the power output of each sensor is tabulated in Table 5.1.

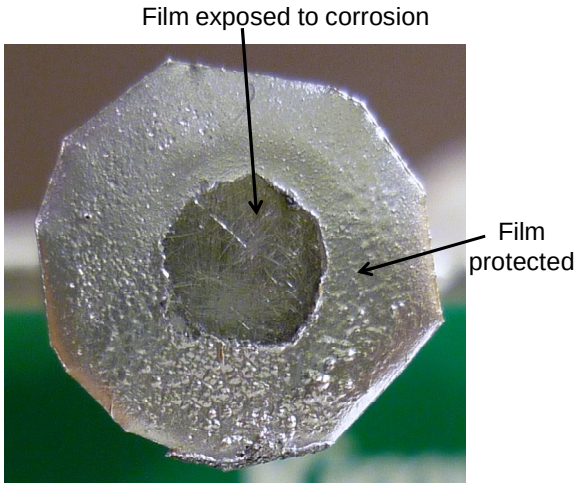

Figure 5.1: Packaged sensor with reduced exposed area.

Table 5.1 Initial power output readings of sensors

Laser output (mW)	P41 (µW)	P42 (µW)	P43 (µW)	P4 (µW)
47.1	7.26	7.10	4.63	18.99

5.1.1 Results and discussions

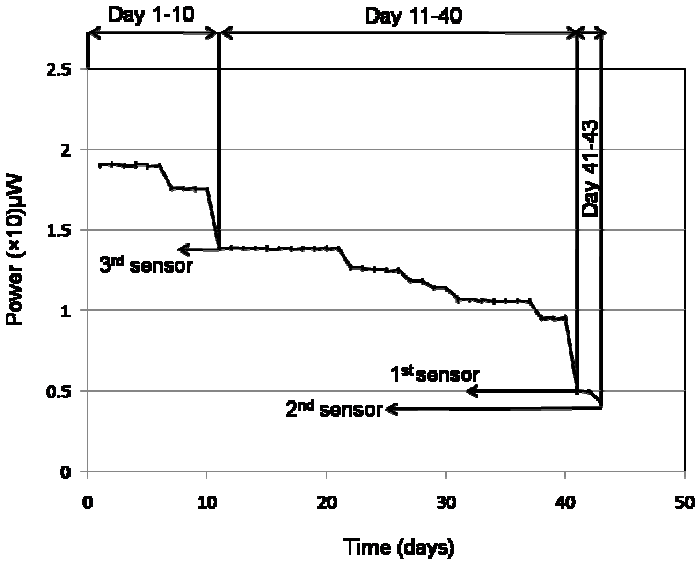

Figure 5.2: Composition of cumulative output over time.

The three packaged sensors were submerged in the 4% saline concentration and its cumulative output was measured on a daily basis. The composition of the cumulative output of

the sensors over 43 days is shown in the Figure 5.2. The cumulative output was steady for 10 days and decreased suddenly by 5 µW indicating that the 3rd sensor detected corrosion as per table 5.1. It was found that the sensor was faulty with water ingress inside the sensor. This faultiness was due to the weld defect that led to the unexpected early failure of the sensor. The cumulative output of the remaining two sensors was then monitored daily as before. On the 40th day, the output of the 1st sensor was decreased by almost half of its initial output (7.26 µW). It was then removed from the measurement system and its percentage change in thickness was found to be 46.3%. On 43rd day, the sensor output of the 2nd sensor was reduced by 3.2 µW (almost half of its initial output). The reduction in thickness for this sensor was 48.7%. Both the 1st and 2nd sensors had almost similar reduction in the material thickness, measured at the time when both of their sensor outputs were reduced by about half of their respective initial output. Figure 5.3 shows the presence of corrosion on the polished side of the film for the 2nd sensor. As only a small area was exposed to the corrosive environment, only the exposed surface (center part of the film) was corroded which can be seen clearly from Figure 5.3. The protected surface of the film was still bright indicating no corrosion on its surface. Hence, this reduction in the exposed area of the sacrificial film overcomes the inconsistent performance of the sensor in terms of material loss.

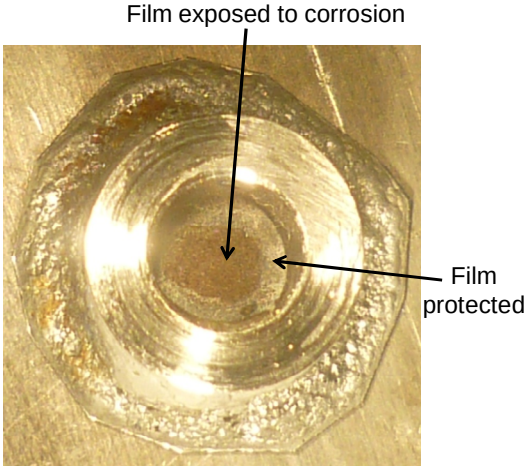

Figure 5.3: Sensor film with corrosion at the center.

5.2 Corrosion sensor with a threaded cap

The main purpose of this experiment was to inspect the changes on the polished surface of the sacrificial film during the corrosion process, whenever a decrease in the sensor power output is observed. Figure 5.4 shows the block diagram and a picture of the threaded corrosion sensor in comparison with a coin showing its actual size. The main difference of this packaged sensor with the sensors described above was that the sensor probe was inserted in and glued to a threaded cap, which was then screw on the tube/film subassembly. The threaded cap enables disassembling the corrosion sensor during the corrosion process to inspect the inner surface of the sacrificial film and the re-assembly of the corrosion sensor after the inspection. Moreover, the thread cap also ensures that the distance between the sensor probe and the sacrificial film is maintained so that the disassembly-reassembly process does not change the sensor output. The repeatability of the sensor position was verified by opening the cap and capped it back a few times. Repeatable sensor output was achieved before and after the disassembly.

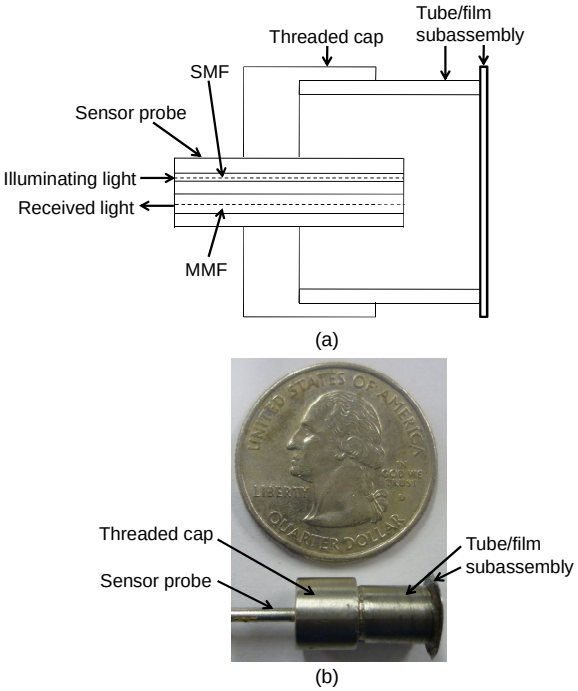

Figure 5.4: Threaded sensor; (a) block diagram; and (b) image of the sensor.

5.2.1 Results and discussions

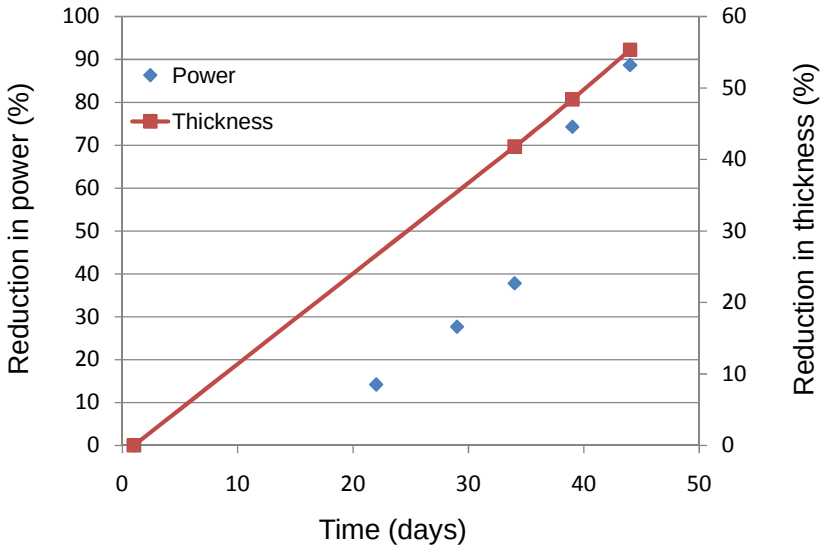

Figure 5.5: Variation of power and thickness percentage with time.

The packaged sensor was submerged in a 4% saline concentration solution. The output of the sensor was measured on a daily basis and its output at the beginning was 68.3 µW. The sensor was disassembled and the percentage change in the film thickness was measured whenever there was a significant decrease in the sensor output. Figure 5.5 shows the variation of percentage reduction in film thickness and the sensor power output with time. The sensor output started to decrease once the corrosion process started to increase the roughness of the polished side of the film. At the early stage, the material loss was small since the corrosion process had just started with fewer corrosion pits. As the exposure time increased, the corrosion pits increased in size and number, leading to rapid increase in the corrosion process. Table 5.2 gives a clear picture of material loss variation with time. The average material loss was 1.23%/day for the first for 34 days and the increase in the corrosion process increased the material loss/day. Figure 5.6 shows the changes of the polished side of the film over time. On day-1, the polished surface of the film was glossy since the corrosion process was not yet started. As the exposure time increases the density of the corrosion pits and the roughness of the film also increased.

Table 5.2 Material loss variation of the film with time

Time (days)	Reduction in sensor output (%)	Change in thickness (%)	Avg. material loss/day (%)
1 - 34	37.80	41.8	1.23
1 - 39	74.30	48.4	1.242
1 - 44	88.69	55.35	1.257

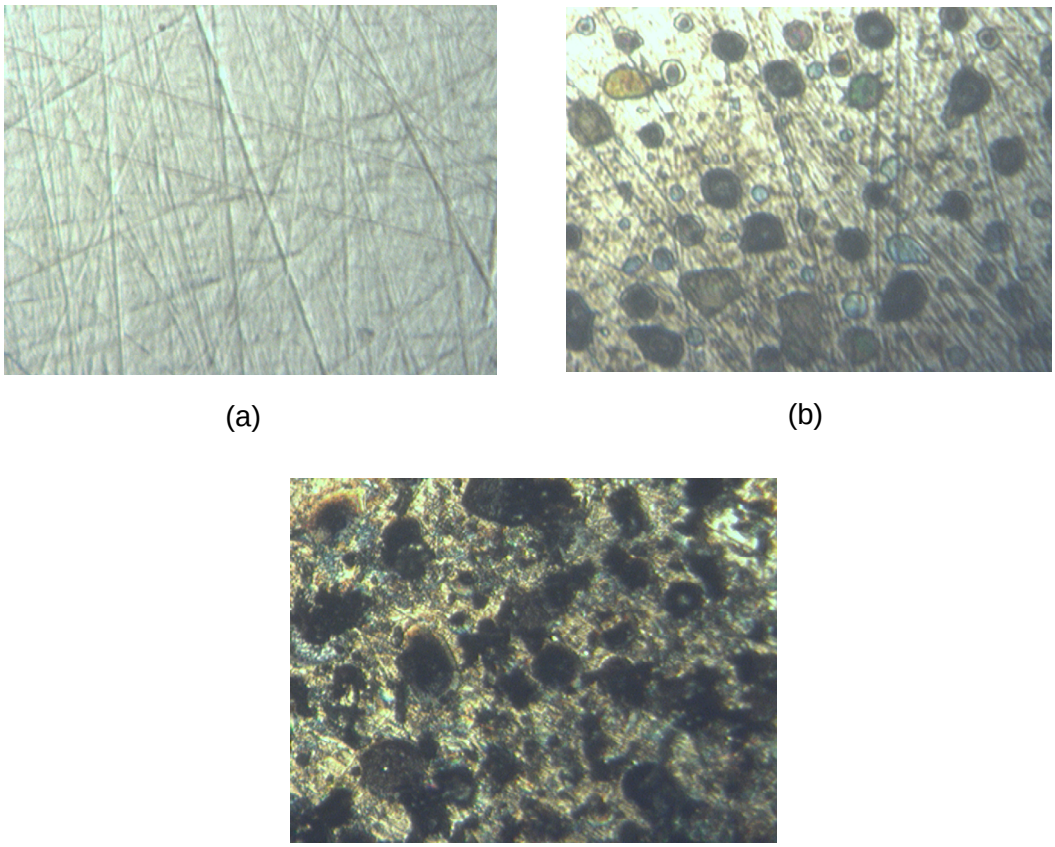

(a) (b)

(c)

Figure 5.6: Changes on the film during corrosion; (a) on day-1; (b) on day-38; and (c) on day-44.

CHAPTER 6

CONCLUSION AND FUTURE WORK

6.1 Conclusion

An innovative technique of detecting corrosion using optical fiber reflectance sensors was investigated. The sensor detects corrosions by monitoring the surface reflectivity changes of a sacrificial metallic film. Bench top tests were performed and validated that the presence of corrosion increases the surface roughness, which in turn decreases the sensor power output significantly. A flexible fabrication technique was developed to package the corrosion sensor in a compact and robust format. The packaged sensors were tested by submerging them in saline solution of different concentrations. Experimental results demonstrated that the corrosion can be detected by the laser reflectance sensor. In the next stage, the exposed area of the sacrificial film was reduced to address the inconsistent performance of the sensor in term of material losses at the time of detection. Experimental results confirmed that the consistent performance of the sensor in terms of material loss can be achieved by reducing the exposed area of the film.

6.2 Future work

The one-direction 4×1 multimode coupler introduces a large insertion loss that reduces the signal-to-noise ratio of the sensor output. In order to minimize this power loss, a multimode fiber bundle embedded in a steel tube connector can be used to replace the multimode coupler. Figure 6.1 shows a general multiplexed setup with a steel tube connector being used instead of the 4×1 MMC. Since the sensing area of the photo-detector is much larger than the fiber area, it can monitor multiple sensor output at the same time, as long as an adaptor is available to accommodate the MMFs and to connect them to the power detector. Since no such an adaptor is available commercially, a customized connector is designed based on the dimensions of the

photo-detector. Figure 6.2 shows the front, top, right and isometric views of the steel tube connector with its dimensions. The sensor outputs of multiple sensors will be aligned inside the adaptor and glued with an optical fiber epoxy. After curing, the adaptor will be polished on aluminum oxide polishing films using the same procedure as that for the sensor probe preparation. Once the adaptor is properly polished, it can be used in the multiplexing setup (see Figure 6.1).

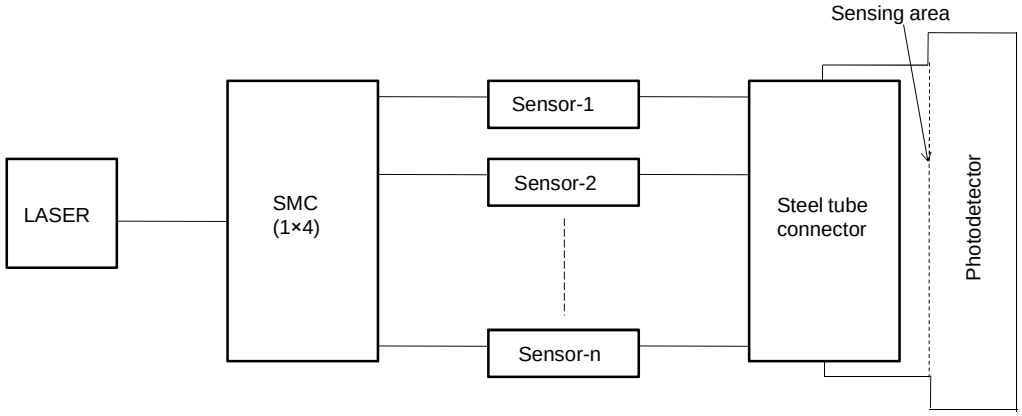

Figure 6.1: General multiplexed setup with steel tube connector.

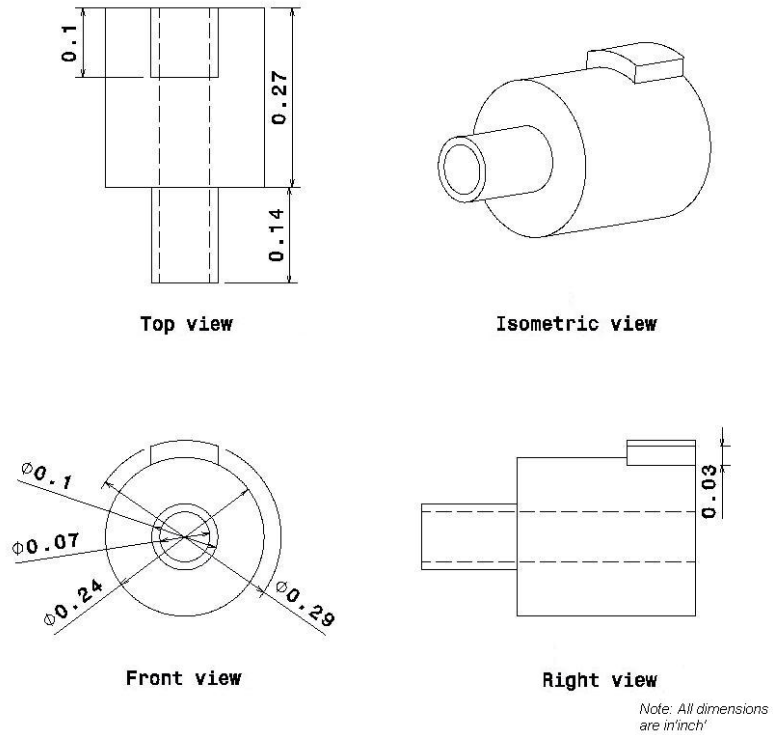

Figure 6.2: Drawing specifications of the steel tube connector.

REFERENCES

1. Trego, A., E.D. Haugse, and E. Udd. *Material removal rate fiber optic corrosion sensor*. 1998. Troutdale, OR, USA: SPIE.
2. Dong, S., et al., *Optical and electrochemical measurements for optical fibre corrosion sensing techniques.* Corrosion Science, 2006. **48**(7): p. 1746-1756.
3. Li, X.M., et al. *Fiber optic corrosion sensor fabricated by electrochemical method*. 1998. San Diego, CA, USA: SPIE.
4. Dong, S., G. Peng, and Y. Luo, *Preparation techniques of metal clad fibres for corrosion monitoring of steel materials.* Smart Materials and Structures, 2007. **16**(Compendex): p. 733-738.
5. Himour, A., et al., *Optical-fiber corrosion sensor based on deposit of Au/Ni-P.* Japanese Journal of Applied Physics, Part 1: Regular Papers and Short Notes and Review Papers, 2005. **44**(Compendex): p. 6709-6713.
6. Cooper, K.R., et al. *Optical fiber-based corrosion sensor systems for health monitoring of aging aircraft*. in *Autotestcom 2001, August 20, 2001 - August 23, 2001*. 2001. Valley Forge, PA, United states: Institute of Electrical and Electronics Engineers Inc.
7. Greene, J., et al. *Optical fiber corrosion sensors for aging aircraft*. in *Process Control and Sensors for Manufacturing, March 31, 1998 - April 1, 1998*. 1998. San Antonio, TX, United states: SPIE.
8. Dong, S., et al. *Optical fiber long-period grating-based Cu[sup 2 +] measurement*. 2005. Shanghai, China: SPIE.
9. Qiao, G., Z. Zhou, and J. Ou. *Thin Fe-C alloy solid film based fiber optic corrosion sensor*. in *1st IEEE International Conference on Nano Micro Engineered and Molecular*

Systems, 1st IEEE-NEMS, January 18, 2006 - January 21, 2006. 2006. Zhuhai, China: Inst. of Elec. and Elec. Eng. Computer Society.

10. Dantan, N., W.R. Habel, and O.S. Wolfbeis. *Fiber optic pH sensor for early detection of danger of corrosion in steel-reinforced concrete structures*. in *Smart Structures and Materials 2005 - Smart Sensor Technology and Measurement Systems, March 7, 2005 - March 9, 2005*. 2005. San Diego, CA, United states: SPIE.
11. Werner, T. and O.S. Wolfbeis, *Optical sensor for the pH 10–13 range using a new support material.* Fresenius' Journal of Analytical Chemistry, 1993. **346**(6): p. 564-568.
12. Kermis, H.R., Y. Kostov, and G. Rao, *Rapid method for the preparation of a robust optical pH sensor.* The analyst, 2003. **128(9)**: p. 1181-1186
13. Mendoza, E.A., et al. *Distributed fiber optic chemical sensors for detection of corrosion in pipelines and structural components*. in *Nondestructive Evaluation of Utilities and Pipelines II, April 1, 1998 - April 1, 1998*. 1998. San Antonio, TX, United states: SPIE.
14. Lo, Y.-L., T.-Y. Yan, and C.-P. Kuo, *Self-referenced intensity-based fiber optic sensor system using fiber Bragg gratings.* Optical Engineering, 2002. **41**(Compendex): p. 1087-1092.
15. Fuhr, P.L., et al. *Fiber optic corrosion sensing for bridges and roadway surfaces*. in *Smart Structures and Materials 1995: Smart Systems for Bridges, Structures, and Highways, Febrary 28, 1995 - March 3, 1995*. 1995. San Diego, CA, USA: Society of Photo-Optical Instrumentation Engineers.
16. Ganesh, A.B., T.K. Radhakrishnan, and G. Gobi, *Estimation of corrosion of metals using fiber optic displacement sensor system.* Sensors and transducers 2006. **70(8)**: p. 645-654
17. Gobi, G., et al., *Laser based optical sensor to observe metal surfaces subjected to early microbic corrosion.* Lasers in Engineering, 2007. **17**(Compendex): p. 397-404.

18. Gobi, G., et al., *Fiber-optic sensor to estimate surface roughness of corroded metals.* Optica Applicata, 2009. **39**(Compendex): p. 5-11.

19. Filho, J.F.M., et al., *optic based corrosion sensor using OTDR.* IEEE, 2007: p. 1-4244-1262-5, 1172-1174.

20. Filho, J.F.M., et al., *Multipoint fiber optic based corrosion sensor*. 2008, SPIE.

21. K.R. Trethewey and J. Chamberlain: "Corrosion for Science and Engineering 2nd Edn.", Longman (UK), 1995.

22. Lee, H.S., et al., *Development of corrosion sensors for monitoring steel-corroding agents in reinforced concrete structures.* Materials and Corrosion, 2003. **54**(Compendex): p. 229-234.

23. Stoecker Ii, J.G., *Microbiological and electrochemical types of corrosion: back to basics.* Materials Performance, 1995. **34**(Compendex): p. 49-52.

24. Singh, B., *Specifying clad CRA piping.* Hydrocarbon Processing, 1993.**72**(Compendex): p. 51-52.

25. J.W. Oldfield: "Electrochemical Theory of Galvanic Corrosion", in "Galvanic Corrosion" - ASTM STP 979 - H.P. Hack Ed., ASTM International, West Conshohocken (PA), 1988.

26. H.P. Hack: "Galvanic Corrosion Test Methods" (Corrosion Testing Made Easy, Volume 2), NACE International, Houston, 1993.

27. Z. Szlarska-Smialowska: "Pitting Corrosion of Metals", Nace International, Houston, 1986.

28. Harrison, C.D. *Basics of fiber optics*. in *Optically Based Methods for Process Analysis, March 23, 1992 - March 26, 1992*. 1992. Somerset, NJ, USA: Publ by Int Soc for Optical Engineering.

29. Caldas, P., et al. *Modal LPG-based Mach-Zehnder interferometer with controlled sensitivity for refractive index measurement*. in *19th International Conference on Optical Fibre Sensors, April 15, 2008 - April 18, 2008*. 2008. Perth, WA, Australia: SPIE.

30. Majumdar, A. and H. Huang, *Development of an in-fiber white-light interferometric distance sensor for absolute measurement of arbitrary small distances.* Applied Optics, 2008. **47**(Compendex): p. 2821-2828.

31. Li, J. and X. Zhong. *Study on optical fiber concentration sensor*. in *15th Congress of the International Commission for Optics, August 5, 1990 - August 10, 1990*. 1990. Garmisch-Partenkirchen, Germany: Publ by Int Soc for Optical Engineering.

32. Bariain, C., et al., *Optical fiber humidity sensor based on a tapered fiber coated with agarose gel.* Sensors and Actuators, B: Chemical, 2000. **69**(Compendex): p. 127-131.

33. Glass Photosensitivity and Fiber Gratings, Fiber Optics Research Center GPI RAN, 2003-04.

34. Huang, H. and U. Tata, *Simulation, implementation, and analysis of an optical fiber bundle distance sensor with single mode illumination.* Applied Optics, 2008. **47**(Compendex): p. 1302-1309.

35. Huang, H., U.S. Tata, and A. Majumdar. *A novel all-fiber surface roughness sensor-based on laser scattering*. in *World Forum on Smart Materials and Smart Structures Technology, SMSST 07, May 22, 2007 - May 27, 2007*. 2008. Chongqing, Nanjing, China: Taylor and Francis/Balkema.

36. Mathworld.Wolfram website: http://mathworld.wolfram.com/Circle-CircleIntersection.html

BIOGRAPHICAL INFORMATION

Manjunatha Shenoy earned his Bachelor of Engineering in Mechanical Engineering from Visvesvaraya Technological University, Belgaum, India, in June 2005. He worked in a multinational design and manufacturing company “Rittal India Pvt. Ltd., Bangalore, India” to gain practical experience before heading towards United States of America for his graduate studies. He was awarded Master of Science in Mechanical Engineering from University of Texas at Arlington in May 2010.